Journal of Materials Chemistry A

High-temperature and water-based evaporation induced self-assembly approach for facile and rapid synthesis of nanocrystalline mesoporous TiO2

Journal:	*Journal of Materials Chemistry A*
Manuscript ID:	TA-ART-06-2014-002912.R2
Article Type:	Paper
Date Submitted by the Author:	29-Jul-2014
Complete List of Authors:	Wang, Wei; Northeastern University, Key Laboratory for Anisotropy and Texture of Materials of Ministry of Education Ruan, Chengdong; Northeastern University, School of Materials and Metallurgy Long, Haibo; Northeastern University, School of Materials and Metallurgy liu, guoqiang; Northeastern University, ; Northeastern University, School of Materials and Metallurgy Li, Song; Northeastern University, Key Laboratory for Anisotropy and Texture of Materials of Ministry of Education Yue, Xinyan; Northeastern University, Key Laboratory for Anisotropy and Texture of Materials of Ministry of Education Ru, Hongqiang; Northeastern University, School of Materials and Metallurgy

Cite this: DOI: 10.1039/c0xx00000x

www.rsc.org/xxxxxx

ARTICLE TYPE

High-temperature and water-based evaporation induced self-assembly approach for facile and rapid synthesis of nanocrystalline mesoporous TiO_2 †

Wei Wang,*[a] Chengdong Ruan,[b] Haibo Long,[b] Guoqiang Liu,[b] Song Li,[a] Xinyan Yue,[a] Hongqiang Ru*[b]

Received (in XXX, XXX) Xth XXXXXXXXX 20XX, Accepted Xth XXXXXXXXX 20XX
DOI: 10.1039/b000000x

Various appealing applications of mesoporous TiO_2 continuously spur the research on related mesostructural design as well as innovation in preparation. This work reports a novel high-temperature and water-based evaporation induced self-assembly (HW-EISA) approach based on a simple ternary templating system (peroxotitanic acid/P123/H_2O), enabling the facile and rapid synthesis of nanocrystalline mesoporous TiO_2 with unusual structures: high surface areas (140-240 m^2g^{-1}), ultra-large mesopores (20-30 nm)/pore volumes (0.7-1.0 cm^3g^{-1}) and tuneable bi-crystallinity (anatase plus rutile). The unusual templating and following decomposition behaviors of P123 were newly unveiled to play crucial and multiple roles in inducing self-assembly between peroxotitanic acid and P123 for final meso-TiO_2 with ultra-large mesopores/pore volumes during the HW-EISA and helping preserve the integrity of mesostructures during calcination, respectively, and rendering the bi-crystallinity in the titania frameworks as well. Other PEO-based nonionic surfactants were also demonstrated to be applicable in producing similar mesostructures. Photocatalytic testing results showed that both high surface areas and the synergistic effect of bi-crystallinity of anatase plus rutile are of great significance in enhancing the photocatalytic properties of meso-TiO_2.

1.Introduction

Mesoporous TiO_2 (meso-TiO_2) materials have attracted enormous attention in recent years due to their promising applications in photocatalysis, water splitting, sensors, solar cells and lithium rechargeable batteries, etc., as summarized in some reviews.[1,2] In view of these applications, mesoporous titania with high surface area, large mesopore/pore volumes and preferentially adjustable crystallinity are highly desirable. Since the first synthesis of mesoporous titania in 1995 *via a* surfactant templating route,[3] extensive efforts have been devoted to the controllable engineering of the titania mesostructures.[1,2] However, some issues so far encountered in the preparation of meso-TiO_2 still concern the researchers: (1) Relatively low thermal stability of mesostructures. Thermal treatments that are widely employed to both induce/improve the crystallization and evacuate the pores often lead to significant deterioration in the mesostructures, reflected by substantial decrease in high surface area. Intrinsic high aptness to sintering of nano-titania being hard to accommodate the curvature of mesopore accounts for this.[2] Therefore, some adjustments to the syntheses have been applied to circumvent this problem,[4] including the addition of glass or glass-like phases to control the crystallization of titania meso-walls,[4a,c,e] the incorporation of hard template scaffold to strengthen the mesostructures,[4b,d] and so on. (2) Small mesopores/pore volumes. Generally, relatively large surface areas are normally obtained in meso-TiO_2 with small mesopore sizes and thin walls, which are similar to the cases of mesoporous silicas and are mainly dependent on the surfactant employed.[3-5] The mesopore sizes are thus rarely over 10 nm.[5] So far, the preparations of meso-TiO_2 with larger mesopores, yet not necessarily leading to large pore volumes,[6] are mainly based on some lab-made surfactants with large molecular weights, e.g., KLE,[6b] PS-*b*-PEO,[6c-d] PI-*b*-PEO,[4b,6e] PMMA-*b*-PEO,[6f] PIB-*b*-PEO,[6g] PVC-g-POEM,[6h-i] necessitating further synthetic steps and expertise. (3) Difficult control over crystallinity. The most often reported phases for meso-TiO_2 are anatase or semi-crystalline (Amorphous plus anatase).[4-7] In some applications such as photocatalysis and lithium ion batteries,[8] rutile phase was also proved to be promising, yet hardly realizable because the thermal-dynamically stable rutile phase is often obtained *via* phase transformation from anatase at even higher calcination temperatures,[9] which might further compromise the mesostructures. It is apparent that certain requirements on both mesoporous and crystalline structures of meso-TiO_2 are actually conflicting to each other, implying that it could be even more challenging to integrate them in one meso-TiO_2. Indeed, according to our literature review, the synthesis approaches that well addressed above-mentioned three concerns have not been reported yet, though many works partially did.

Current problems and demands in manipulating the structures of meso-TiO_2 aside, the synthesis approaches for meso-TiO_2 themselves also turn out to be much less versatile than those for

meso-silicas. Compared with some solution-based synthesis approaches reported so far,[3,6a,10] the evaporation induced self-assembly (EISA) approach was predominantly employed to prepare meso-TiO_2 on account of at least two reasons[1,2,4,6b-g]: (1) The hydrolysis and condensation reaction of highly reactive titanium precursors, mainly the alkoxides and chlorides, can be well regulated by controlling the amounts of water, acidity, etc. (2) The EISA process between the inorganic titanium hydroxides or oligomers and surfactant secures the evolution of mesostructures conveniently, and ordered mesostructures can also be preserved against calcination under delicate control over a series of synthetic variables, including pH values, water content, humidity, thermal treatment parameters, etc. However, the EISA process, in principle, still shows to be a low temperature (≤60 ^oC),[4,5b-5i] more apolar solvent-based (e.g., ethanol, tetrahydrofuran) [4,5b-i,6b-g] and slightly time-consuming (one day ~ several weeks [4,5,7,10]) synthesis approach for either ordered or disordered meso-TiO_2, necessitating careful control over synthetic variables, which could add to the complexity of the synthesis of meso-TiO_2.

Addressing the above research concerns over both the structural manipulation and synthesis procedure, this work reports a novel high-temperature and water-based evaporation induced self-assembly (HW-EISA) approach based on a simple ternary templating system (peroxotitanic acid/P123/H_2O), leading to meso-TiO_2 with unusual structures: high surface areas, ultra-large mesopores/pore volumes and tunable bi-crystallinity (anatase plus rutile, i.e., A+R). The peroxotitanic acid (PTA) and its sol-gel control [11], though has been employed to prepare TiO_2 with different structures,[12] including particles, titania composites, films, etc., have not been demonstrated in the preparation of mesoporous TiO_2. In this work, the syntheses were conducted by directly evaporating at 100 ^oC the aqueous solution containing PTA and commercially available surfactant (P123), the former of which was firstly demonstrated in this work to be a suitable and easy-handling inorganic building species for meso-TiO_2 *via* self-assembly process with surfactant. In addition, two appealing characteristics about the HW-EISA are: (1)The evaporation of water was conducted at as high temperature as 100 ^oC, allowing fast preparation: the total time taken to prepare as-dried PTA/P123 hybrid bulk materials ready for calcination from raw materials, namely titanyl sulfate, can be shortened to be ~3 h. (2) The HW-EISA is a pure water-based and acid-free templating system and therefore is more environment-friendly. In the following context, four specific issues will be sequentially elucidated:

1） What kind of unusual mesostructures for meso-TiO_2 can be obtained *via* the HW-EISA?

2） How do such mesostructures result, especially the roles of P123 in HW-EISA?

3） Some other appealing characteristics about HW-EISA approach itself.

4） What performances can such meso-TiO_2 display as photocatalyst?

2. Experimental

2.1 Chemicals. Titanyl sulfate ($TiOSO_4 \cdot xH_2O$) and Pluronic PEO_{20}–PPO_{70}–PEO_{20} (P123 with Mn = 5800) were purchased from Aldrich. Ammonia ($NH_3 \cdot H_2O$, 35% in H_2O) and hydrogen peroxide (H_2O_2, 30% in H_2O) were purchased from the Sinopharm Chemical Reagent Co., Ltd. All the chemicals were used as received.

2.2 Mesostructure preparation. In the preparation, the titania hydroxide was initially prepared by precipitating the Ti^{4+} using $NH_3 \cdot H_2O$, and then peptized by H_2O_2 to form a peroxotitanic acid (PTA) sol. Typically, titanyl sulfate (8.0 g) was dissolved in doubly de-ionized water (250 ml) to form a clear solution at 40 ^oC under stirring. After being cooled to 25 ^oC, ammonia was added dropwise to adjust the pH value to ~7 under stirring. The titania hydroxide precipitation was collected by centrifugation and washed by copious de-ionized water. To prepare a clear sol of PTA, freshly prepared titanium hydroxide precipitate was added to the solution of hydrogen peroxide (45.0 g, 30% in H_2O) and de-ionized water (15.0 g) under vigorous stirring. In about half an hour, red-yellow colored clear PTA sol formed (**Note:** Temperature should be controlled to be lower than 20 ^oC to avoid rapid gelation of PTA, and the H_2O_2 should be handled with care). The clear sol was continuously stirred for some time to allow the decomposition of H_2O_2. In a typical preparation of mesoporous titania, PTA sol (10.0 g) was mixed with P123 solution (6.0 g, 10 % w/w) to form a clear homogeneous solution (~2mm thick) in an open disc, which was then directly transferred to 100 ^oC oven for 2 h (No boiling observed throughout the process due to the presence of PTA and P123). The obtained PTA/P123 bulk materials were subject to calcination at 450 ^oC in air for 2 h with the heating ramp of 1.5 ^oC/min to both crystallize the titania and evacuate the mesopores. The eventually obtained mesoporous titania was designated as P6/450, where 'P6' denotes relative amounts of P123 solution with respect to PTA sol, and '450' for the calcination temperature. Other namings can be deduced by analogy.

2.3 Structural characterization. Powder XRD patterns at 2θ angles from 15° to 80° for wide angle and from 0.6 to 3° for low-angle were recorded on a Bruker D8 diffractometer using Cu Kr radiation (40kV, 120mA). The phase contents of meso-TiO_2 can be calculated based on the integrated intensities of anatase (101) and rutile (110), respectively according to Zhang, *et al.*[13] The crystal size of nanocrystalline TiO_2 was estimated by applying the Scherrer equation.[14] TEM and high-resolution TEM (HR-TEM) measurements were performed using a JEM2100F instrument operated at 200 kV. FE-SEM images were recorded using scanning electron microscope (Hitachi, S-4800) on samples without any conductive coating. The low operation acceleration voltage and height between detector and sample were used to guarantee quality imaging. TGA-DTA analyses (NETZSCH STA 449F3) were carried out in air with heat ramp of 10 $^oCmin^{-1}$ from room temperature to 800 ^oC. Nitrogen adsorption isotherms were measured at -196 ^oC using Autosorb iQ Station 1 analyzers manufactured by Quantachrome Instruments. The specific surface areas of the samples were calculated using the BET method. The pore size distributions (PSDs) of the cell pore and window pore were determined based on the adsorption and desorption branches using the BJH model for cylindrical pores, respectively.[15] According to the pore shapes of meso-TiO_2 reported below, the pore size distributions should be determined using the BDB method with the film thickness (t) calibrated for spherical pores.[16]

However, considering the facile comparison with pore sizes reported by others and the small differences between pore sizes derived from BJH method and BDB method (Table S1, Electronic Supplementary Information, ESI†), the BJH method derived PSDs were employed. The total pore volume was estimated from the amounts of N_2 adsorbed at a p/p^0 ~0.995.

2.4 Photocatalytic activity test. The photo-degradation of the xanthene dye Rhodamine B (RhB) was carried out in a cylindrical flask as a photo-reactor. Meso-TiO_2 (5.0 mg) was stirred in RhB aqueous solution (20 ml, C_0=1.1×10^{-5} mol/L). Continuous stirring in the dark for 30 min allows reaching the adsorption equilibrium of Rhodamine B with the catalyst. The solution in the flask was irradiated by a 500 W mercury lamp in a cold trap equipped with 365 nm UV filters. The degradation rate was determined at 30 mins intervals by UV-Vis absorption at 550 nm using a UV-Vis Spectrometer (PG2000-Pro-EX, Fuxiang, China). The photocatalytic decomposition of RhB is found to be a pseudo-first-order reaction, and its kinetics may be expressed as follows: $\ln(C^0/C) = kt$,[17] where k is the apparent reaction rate constant (min^{-1}), C^0 and C are the initial concentration and reaction concentration of RhB, respectively.

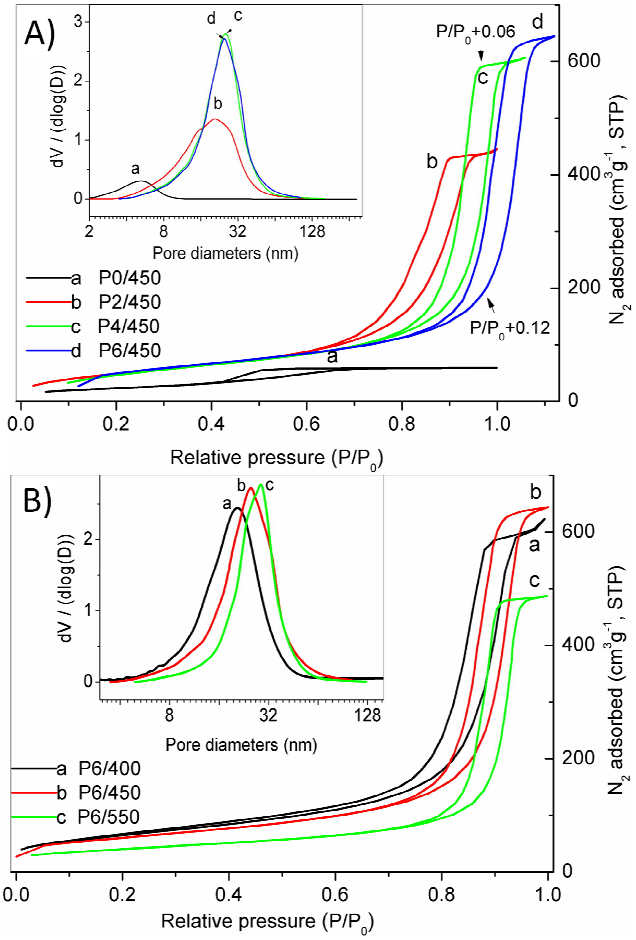

Fig. 1 N_2 adsorption-desorption isotherms and corresponding pore size distributions (PSDs) of meso-TiO_2 prepared with (A) varying amounts of P123 after calcination at 450°C and (B) fixed amount of P123 but varying calcination temperatures. In (A), isotherm curves of *c* and *d* were shifted horizontally by +0.06 and +0.12 to avoid overlap, respectively.

3. Results and discussion

3.1 Unusual Mesostructures of meso-TiO_2 *via* HW-EISA

Fig. 1A shows the N_2 sorption results and corresponding pore size distributions (PSDs) of meso-TiO_2 calcined at 450°C, with detailed textural data shown in Table 1. All N_2 adsorption-desorption curves of P2, 4, 6/450 prepared with increasing amounts of P123 show type IV isotherms with huge and steep capillary condensation/evaporation steps at p/p^0 over 0.9, indicating the presence of uniform and large mesopores and pore volumes as well. The presence of narrow H_1-type hysteresis loops also indicates the formation of unconstricted mesopores. In contrast, the titania prepared without P123 (P0/450, Fig. 1a, curve a) shows significantly lower N_2 uptake, indicating the formation of poor mesostructures, which were actually confirmed to arise from the random packing of titania crystals according to the FE-SEM observations shown in Fig. 2a. The PSDs calculated by BJH method based on adsorption branches are shown to increase with the amounts of P123 up to 25.4nm for P4/450 and reach a plateau upon further increase to 25.5nm for P6/450. Nearly the same trend can also be observed from the evolution of surface areas: sharply increase from 86 m^2g^{-1} (P0/450) to 197 m^2g^{-1} (P4/450) and further but slightly to 212 m^2g^{-1} (P6/450), as listed in Table 1. The mesopore sizes are the largest one ever achieved based on P123 surfactant alone. Associated with the large mesopores, the unprecedentedly high pore volumes reach 0.97 and 1.02 cm^3g^{-1} for P4/450 and P6/450, respectively. Apparently, P123 plays a key role in directing the formation of the mesostructures of meso-TiO_2, suggesting that P123 in the HW-EISA approach, although still acts as an organic template similar to that reported in conventional EISA approach, might exhibit significantly different templating behaviors that are responsible for the formation of such ultra-large mesopores and pore volumes. This will be elaborated in section 3.2.

Apart from the influence of P123, the calcination temperatures were also found to have great influence on the structures of meso-TiO_2. Compared with P6/450 (212 m^2g^{-1}), P6/400 shows slightly higher surface area (235 m^2g^{-1}), while further increase in the calcination temperature to 550 °C led to a modest drop in the surface area to 143 m^2g^{-1} and pore volume of 0.77 cm^3g^{-1} for P6/550, indicative of the excellent thermal stability of TiO_2 mesostructures obtained (Fig. 1B and Table 1).

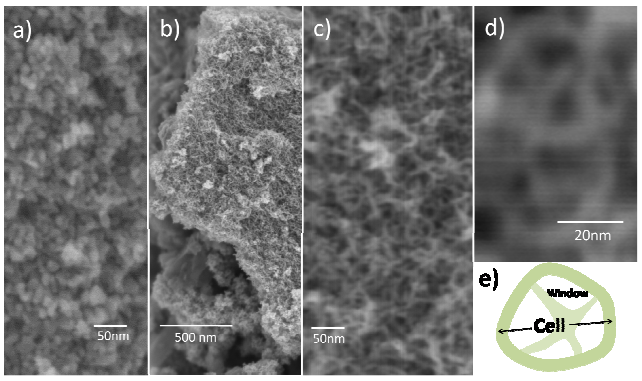

Fig.2 Representative FE-SEM images of (a) P0/450 and (b-d) P6/450 at different magnifications. (e) A schematic of one cell pore and its window pores.

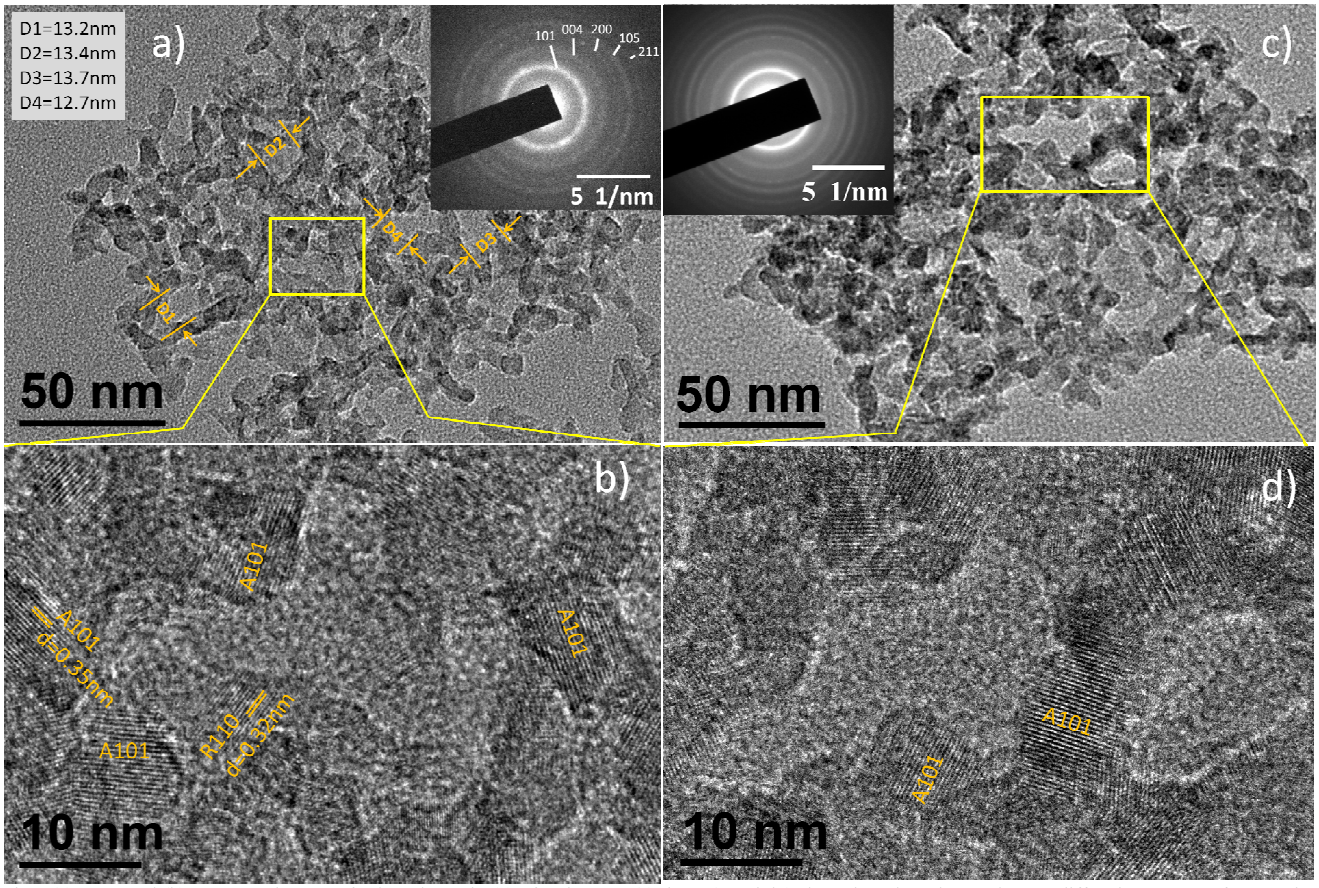

Fig.3 (a) TEM and (b) HR-TEM images of selected area in (a) of P6/400. In (a), inset (top right) show the selected area electron diffraction pattern of meso-TiO_2; Inset (top left) list shows the discernible window pore sizes marked in TEM image shown in (a). In (b), some anatase ('A') and rutile ('R') nanocrystals were labelled. (c) and (d) are TEM and HR-TEM images of selected area of P6/450.

Table 1 Properties of meso-TiO_2 obtained *via* HW-EISA [a)]

Samples	BET/m^2g^{-1}	V/cm^3g^{-1}	D_a/nm	D_d/nm	A_R/%	W_A/nm	W_R/nm
P0/450	86	0.09	5.4	4.2	0.0	19.8	--
P2/450	183	0.73	20.5	16.1	10.6	6.8	7.5 [e]
P4/450	197	0.97	25.4	15.9	15.2	6.3	4.8
P6/450	212	1.02	25.5	15.6	20.2	6.5	4.2
P0/550	41	0.06	8.9	4.5	0.0	23.8	--
P6/550	143	0.77	29.0	19.0	25.9	8.8	8.1
P6/400	235	0.99	20.9	14.1	14.1	5.7	5.0

a): V is the total pore volume. D_a and D_d are the BJH pore size calculated based on adsorption and desorption branches, corresponding to the cell and window pore sizes respectively, as depicted in Fig. 2e. A_R is the phase contents of rutile in weight percent, the rest is anatase, that is (100-A_R)%. W_A and W_R are the anatase and rutile crystal sizes calculated by Scherrer equation, respectively.

FE-SEM images shown in Fig. 2b-d directly show that the uniform mesostructures of bulk pieces of meso-TiO_2 (P6/450) samples after calcination prepared *via* HW-EISA are one kind of 3D-interconnected cellular sponge structures with thin 'struts' of less than 10 nm, which can be schematically depicted in Fig. 2e. Such mesostructures are significantly different from those of P0/450 (Fig. 2a) prepared in the absence of P123. The thin 'struts' also mean that the titania crystal sizes are very small, correlating with the high surface area of P6/450. The cell sizes and window pore sizes are estimated to be in the range of 20-30 nm and 10-20 nm, respectively, which are also in agreement with those estimated by BJH method from the adsorption and desorption branches (Table 1), respectively. According to the FE-SEM images shown in Fig. S1 (ESI†), P2/450 and P4/450 show similar mesostructures with those of P6/450 (Fig. 2b-d), consistent with the N_2 sorption results shown in Fig. 1 and Table 1. The low-angle XRD pattern of P6/400 (Fig.S2, ESI†) shows to be featureless: no low-angle peak can be found, which can be attributed to either the large d-spacings due to the large pore size beyond the testing limit of diffractometer or the broadened pore size distributions, or both.

TEM images of P6/400 shown in Fig. 3a-b also corroborate above N_2 sorption results on mesostructures: interconnected mesostructures with large mesopores were formed. The discernible pores (that more probably are window pores in TEM measurement, Fig. 3a) are averaged to be around 13.3 nm, which agree well with N_2 sorption results. Selected area electron diffraction pattern shown in Fig. 3a (top right) also demonstrated that the meso-TiO_2, even after calcination at low temperature of 400 °C for 2 h, shows to be highly crystalline anatase phase. High resolution TEM image (Fig. 3b) further confirms that the 'struts' or pore walls are composed of TiO_2 nanocrystals with sizes less than 10 nm. Interestingly, other than anatase phases, the 'struts' are also found to be decorated by sporadic rutile nanocrystals, which were also confirmed by below wide-angle XRD results.

Not surprisingly, P6/450 also shows high crystalline mesostructures with large interconnected mesopores, as can be seen from the TEM results (Fig. 3c-d) and the SAED image (Fig. 3c, inset). More TEM and HR-TEM images can be found in supplementary data (Fig.S3, ESI†). Higher calcination temperature at 450 °C clearly did not change the mesostructures substantially.

In terms of both the large mesopore size and disordering, such obtained mesostructures resemble those prepared using lab-made block copolymers (PI-*b*-PEO, with high molecular weight ~84.4K) as template, as reported by Nedelcu et al.[6e] However, the surface areas of those meso-TiO_2 are as low as 30-40 m^2g^{-1} due to the formation of thick walls, which are significantly different from the meso-TiO_2 with sub-10 nm nanocrystalline walls reported here based on commercial P123 with much lower molecular weight (M_n~5.8K) under HW-EISA conditions.

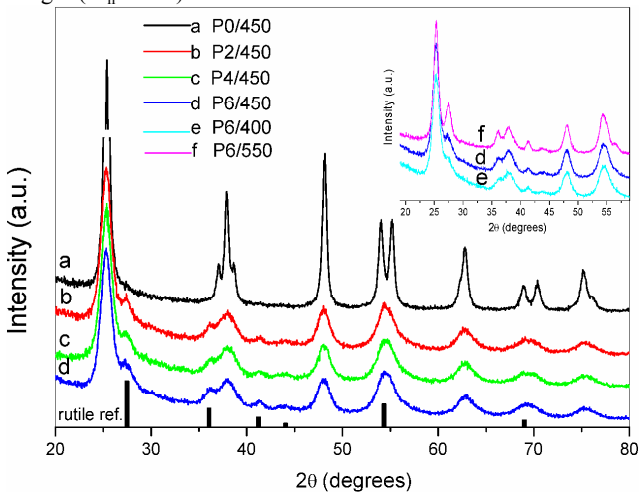

Fig. 4 Wide-angle XRD patterns of meso-TiO_2 prepared with (a-d) varying amounts of P123 after calcination at 450 °C and (d-f, inset) fixed amount of P123 but varying calcination temperatures. The rutile reference (ICDD PDF2 00-004-0551) was also provided to differentiate the reflections of rutile from those of anatase.

Fig. 4 shows the wide-angle XRD patterns of some meso-TiO_2 shown in Fig. 1 and Table 1. Clearly, all meso-TiO_2 prepared with P123 show the bi-crystallinity, namely the mixture of the dominant anatase phase and small proportions of rutile phase. The proportions of rutile (10.6→20.2%, and the rest is anatase) increase with the increasing amounts of P123 from P2/450 to P6/450. The same trend can be observed with the increase in calcination temperatures (14.1 % for P6/400→25.9 % for P6/550). In contrast, P0/450 shows to be mono-crystalline anatase and even after calcination at 550 °C for 2 h (Fig. S4, ESI†). Therefore, P123 does play a crucial role in inducing the formation of rutile phases and thus the bi-crystallinity in meso-TiO_2, which is consistent with some similar results on the crystallization of TiO_2 particles prepared from PTA in the presence of polyethylene glycol additives.[18] The crystal sizes of the primary anatase phase are estimated to be 6-7 nm by the Scherrer equation after calcination at 400 or 450 °C and gently increases to 8.8nm after calcination at 550 °C (Table 1), which agrees well with the observations of FE-SEM (Fig. 2b-d) and HR-TEM (Fig. 3).

Assuming TiO_2 particles in a hard sphere model,[19] the BET surface areas of loose TiO_2 powders, S (m^2g^{-1}) =6000/(ρ*D*), where ρ and *D* are the density (cm^3g^{-1}, 3.86 g/cm^3 for anatase) and diameter (nm) of the spherical particle, respectively. The BET surface areas of TiO_2 particles with size of 6-9 nm can reach around 259-172 m^2g^{-1}. Such values are consistent with measured ones of meso-TiO_2 shown in Table 1, implying again the intactness of mesostructures as well as high thermal stability against sintering of well-defined TiO_2 mesostructures thus obtained.

3.2 Unusual and multiple roles of P123 in templating and decomposition in HW-EISA

Considering the ultra-large mesopores/pore volumes of meso-TiO_2 obtained *via* the HW-EISA reported here, the micelles of P123, though functions similarly in templating the inorganic building species, are believed to possess much larger micellar sizes than those of P123 previously attempted for meso-TiO_2 and -silicas.[5b-g,20] Normally, in order to secure the meso-orderings, the self-assembly process is normally conducted at relative low temperatures in the range of 10-60 °C,[4,5,7,10,21] where common ordered hexagonal/cubic phases appear at a wide range of P123 concentrations according to the phase diagram of P123 in water.[22] In this work, the HW-EISA syntheses were directly conducted at 100 °C, and under such conditions the P123 micellar aggregates tend to grow significantly with the increase in the temperature according to literature: the diameters of spherical micelles increase from 11.6 nm at 25 °C to 17.4 nm at 45 °C.[22] On the other hand, the increased hydrophobicity of the PEO segment at such temperatures also increases the hydrophobic core sizes[21,23] and thus accounts for the formation of meso-TiO_2 with ultra-large mesopore sizes in this work. In order to further attest this explanation, meso-TiO_2 were prepared with the same conditions (P6/450) but at low EISA temperatures, i.e., 40 and 55°C, as controls (Fig. 5A). The mesopore sizes are 13.7 nm (P6/450 with EISA @40 °C) and 16.6nm (P6/450 with EISA @55 °C), which are significantly smaller than 25.5 nm of P6/450 prepared by HW-EISA process at 100 °C. The much smaller mesopore size of P6/450 (EISA @ 40 °C) was also confirmed by the FE-SEM image shown in Fig. 5B-C. Such mesopore size of 13.7 nm is very close to our previous reports on meso-silicas prepared using P123 as template under proper hydrothermal treatments.[24] Clearly, the higher the temperature the EISA process was conducted, the larger the mesopore of meso-TiO_2 will be. This is consistent with above discussion and strongly supports that the high temperature (i.e., 100 °C) employed in the HW-EISA approach did play a key role in producing meso-TiO_2 with ultra-large mesopores/pore volumes based on the self-assembly between P123 and PTA.

In order to further investigate the universality of HW-EISA approach in delivering similar mesostructures (e.g. the large mesopores and pore volumes), three other often used PEO-based nonionic surfactants were also attempted, i.e., Brij56 ($C_{16}EO_{10}$, M_n~683)), L64 ($EO_{13}PO_{30}EO_{13}$, M_n~2900) and F127 ($EO_{106}PO_{70}EO_{106}$, M_n~12600). As shown in the FE-SEM images in Fig. 5D-F, Fig. S5-6 and Table S2 (ESI†), the obtained meso-TiO_2 show some expected characteristics: (1) All the mesopore sizes templated by these surfactants *via* HW-EISA approach are all much larger than those of meso-TiO_2 ever prepared:13.8 nm, 19.7 nm and 25.4 nm for Brij56, L64 and F127 templated meso-TiO_2, respectively. In our and others' work,[21b,25] the pore size of mesoporous materials templated by Brij56 and L64 are all in the

range of 2~9 nm, and F127 normally leads to comparable mesopore sizes (<10 nm) to those by P123.[5d, l, 21b] (2) The pore sizes are still correlated well with the molecular weights of the hydrophobic components in these surfactants. For example, the mesopore size of meso-TiO_2 templated by Brij56 is 13.8 nm, while the larger and comparable mesopores of meso-TiO_2 templated by P123 and F127 are close to each other (~25.5 nm). This, from the other side, proves that the formation of mesostructures are strongly depending the interplay between the PTA species and surfactants. Other PEO-based nonionic surfactants are therefore demonstrated to be applicable in such ternary PTA/P123/water system to yield similar and adjustable structures of meso-TiO_2.

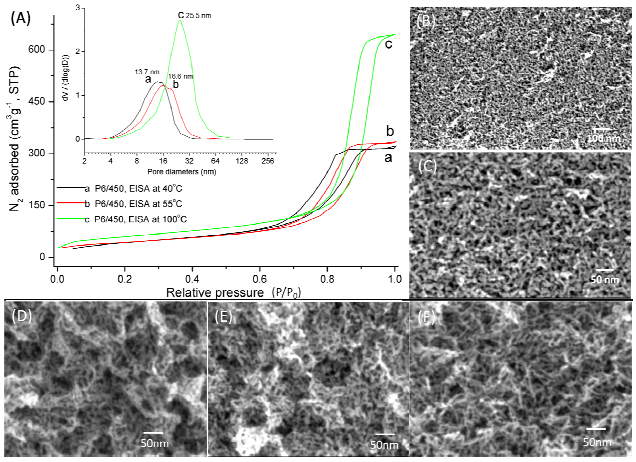

Fig. 5 (A) N_2 adsorption-desorption isotherms and corresponding pore size distributions (PSDs, left inset) of calcined meso-TiO_2 prepared *via* EISA process carried out at (a) 40 °C, (b) 55 °C (The dryings of the PTA/P123 mixed sol at 40 and 55 °C were extended to 1 day) and (c)100 °C of P6/450, which in included here for comparison purpose only. (B-C) FE-SEM images of P6/450 with evaporation temperature at 40 °C. (D-F) FE-SEM image of Brij-56, L64 and F127 templated meso-TiO_2 under the same conditions with P6/450, respectively.

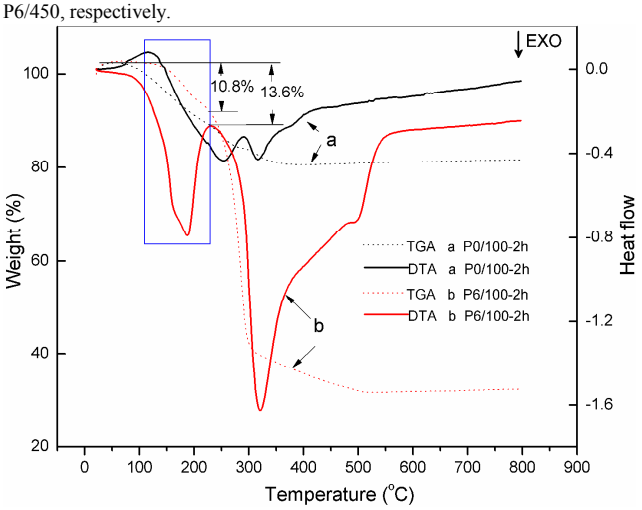

Fig. 6 TGA-DTA analyses of as-dried (a) P0/100-2h and (b) P6/100-2h. The squared area shows the unusual decomposition behavior of P123 at low temperature of P6/100-2h.

During the calcination to evacuate the mesopores, we also found an interesting decomposition behavior of P123 in the presence of PTA: a low-temperature 'decomposition' stage of P123, yet more like a polymerization process, starts at as low as 100 °C and gets prominent at 185 °C, evidenced by a big exothermic peak associated with slight weight loss for P6/100 (10.8 wt.%) compared with pure PTA (13.6%) (Fig. 6). This might be due to the oxidative environment created by the gradual decomposition PTA, causing complex decomposition/polymerization (upon heating) of P123 and its organic derivatives. The black colour of the meso-TiO_2 appears after long-time heating (e.g., 12 h) at 100 °C and persists even after calcination at 350 °C, indicates the presence of carbon species. Such decomposition behavior of P123 is significantly different from those reported in synthesis of SBA-15 meso-silica [21b] and meso-TiO_2 based on other titanium precursor.[5f,g] More importantly, the carbon lining of the mesopores are also believed to be responsible for the excellent thermal stability already observed for meso-TiO_2 shown in this work. Such carbon-strengthening strategy has been demonstrated by different groups in works employing either highly carbonizable organic templates or specially designed carbonization step of surfactant.[4b-d,6b-f]

3.3 Some other appealing characteristics about HW-EISA approach

It should also be pointed out that the HW-EISA system based on PTA was purely water-based and acid-free, which is greatly different from the conventional EISA conducted in more apolar solvents (e.g., ethanol, THF, etc.), while only limited amounts of water, either from moisture in air or by direct addition, were used to hydrolyze the titanium precursors and promote their interaction with the hydrophilic head groups of surfactant. Additionally, in many cases, strong acidic conditions were often employed to reduce the poly-condensation reaction of TiO species, because the protonated hydroxyl groups in the hydrolyzed TiO species can hinder the nucleophilic attack toward positively charged Ti ions and thus retard their poly-condensation reaction. Therefore, to avoid rapid and uncontrollable hydrolysis and condensation of titanium precursor is always the main concern in the conventional EISA process.[4,5b-i,6f] In this work, the PTA sols themselves are sufficiently stable against gelation due to the stabilizing effect of peroxo ligands on PTA species,[26] which allows the EISA process to be accomplished at high temperatures (100 °C) within a short time (~3h) and simultaneously avoids uncontrollable condensation reactions (e.g. rapid precipitations). According to TGA/DTA analysis (Fig. 6), complete elimination of peroxo ligands needs as high temperature as 250 °C. This can also be indirectly seen from the formation of gel-like as-dried P123/PTA hybrid materials, where condensation reaction between PTA species should be sufficiently slow. This explains why the HW-EISA process can be conducted at high temperature and does not need complicated sol-gel control.

In addition, it is also believed that the HW-EISA synthetic strategy for mesostructural manipulation reported here might possibly be extended to prepare a range of mesoporous transition metal oxides (W, V, Mo, Nb, Ta, etc.), as their corresponding precursors can also form similar peroxo-complex species with H_2O_2. Of course, to fully substantiate this, further works are needed.

3.4 Photocatalytic performance of meso-TiO_2

With respect to the photocatalytic properties of meso-TiO_2 in oxidizing organic pollutants in water, many researchers are rather

unanimous on the positive role of high surface area and high crystallinity of anatase, yet still argues about the role of rutile phase: whether or not proper amounts of rutile phase combined with primary anatase phase can enhance the charge separation and hence improve the efficiency of utilization of electron–hole pairs in photocatalysis.[27] In this work, the quality mesostructures and the varying bi-crystallinity of meso-TiO_2 allow us to study the photocatalytic performance of meso-TiO_2, especially the role of rutile phase and the bi-crystallinity, because the P2-6/T series of meso-TiO_2 possess similar mesostructures, such as large pore sizes and TiO_2 nanocrystal sizes, but varying rutile contents relative to anatase (Table 1). The photocatalytic activities for resulting meso-TiO_2 were evaluated in the photo-degradation test of Rhodamine B in water under UV light irradiation (365 nm). Not surprisingly, high-surface-area meso-TiO_2 (P2-6/T) show doubled or even tripled photo-activities compared with P0/450 possessing the lowest surface area (Fig. 7 and Table S3, ESI†). Especially for P2-6/T series of meso-TiO_2, the normalized pseudo-first-order rate constants (k) to surface area for meso-TiO_2 with higher A_R (especially for P6/550 with A_R=25.9%) show superior photocatalytic properties over its counterparts with lower A_R (Table 1, S3 & Fig. S7, ESI†). Therefore, a previously reported synergistic effect between anatase and rutile on enhancing the photocatalytic properties of TiO_2[8a-b] is confirmed to exist for meso-TiO_2 prepared in this work too. This conclusion is believed to be convincible, because meso-TiO_2 samples (P2-6/T series) that were used for comparison possess close mesopore sizes and nanocrystal sizes (Table 1). The HW-EISA approach derived meso-TiO_2 with unusual structures, including high surface areas, unblocked ultra-large pore sizes and especially the tuneable bi-crystallinity, might provide new visions and possibilities in designing meso-TiO_2 with significantly enhanced the photocatalytic properties, which deserves further in-depth exploration in the future.

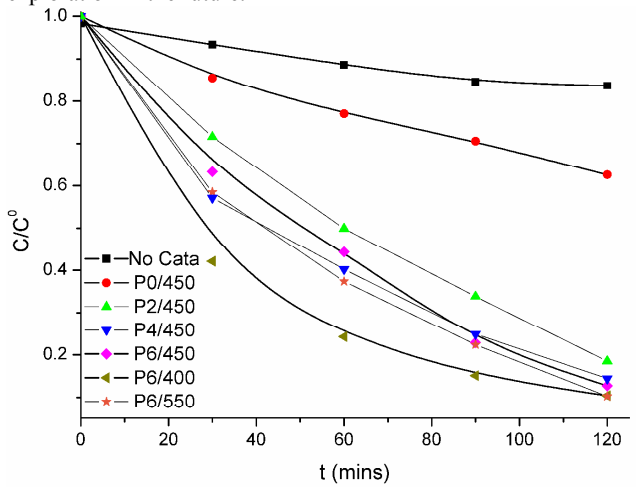

Fig. 7 Photocatalytic degradation of Rhodamine B monitored as the concentration change versus irradiation time in the presence of meso-TiO_2

4. Conclusions

In conclusion, the HW-EISA approach reported in this work constitutes a facile and rapid synthesis protocol based on a simple ternary templating system (PTA/P123/H_2O), allowing the preparation of nanocrystalline meso-TiO_2 with high surface area, ultra-large mesopores/pore volumes and tuneable bi-crystallinity (A+R). The unusual and multiple roles of P123 in templating PTA, its carbonaceous derivative strengthening the mesostructures against calcination and inducing the bi-crystallinity functioned well in harmony to harvest and harness above-mentioned structural properties. The extension of such synthesis from P123 to other PEO-based nonionic surfactants produced similar mesostructural features. Especially, no complicated control over either the hydrolysis/condensation of titanium precursor, or the EISA process between PTA and P123, or the tuning of the bi-crystallinity (Anatase *&* Rutile) is necessary, including pH, water content, additives, humidity control, lengthy time, etc. The photocatalytic testing confirmed that, other than the surface area, the synergistic effect of bi-crystallinity (A+R) does play its role in enhancing the photoactivity of meso-TiO_2 in decomposing Rhodamine B in water. Meso-TiO_2 based on the HW-EISA with even higher photocatalytic properties can be envisaged. Such interesting structural characteristics, which have not been integrated in one meso-TiO_2 before, might be also very useful for applications, where co-catalyst/sensitizer loading and high mass transfer are in demand, e.g. in photocatalysis, lithium ions battery, dye-sensitized solar cell, etc.

Acknowledgment

This work was supported by the National Natural Science Foundation of China (Grant No.21201030, 51272039), and the State Key Program of National Natural Science of China (Grant No. 51032007), the Fundamental Research Funds for the Central Universities (N120410001 and N100702001) and Liaoning Province Innovation Funds (2014020030). We thank the help from Weijun Shan for low-angle XRD measurements.

Notes and references

[a] *Key Laboratory for Anisotropy and Texture of Materials of Ministry of Education (ATM), Northeastern University, Shenyang110819, PR China; Tel: +86-24-83680248; E-mail: wangw@atm.neu.edu.cn*
[b] *School of Materials and Metallurgy, Northeastern University, Shenyang 110819, PR China. Tel:+86-24-83680248;E-mail: ruhq@smm.neu.edu.cn*

† Electronic Supplementary Information (ESI) available: (Table S1) Cell and window pore size distributions derived from BJH (cylindrical pore) and BDB (spherical pore) methods. (Fig.S1) FE-SEM images of P2/450 and P4/450 at different magnifications. (Fig.S2) Low-angle XRD pattern of P6/400. (Fig.S3) TEM and HR-TEM images of P6/450. (Fig.S4) Wide-angle XRD pattern of P0/550. (Table S2) Properties of meso-TiO_2 obtained *via* HW-EISA prepared with other PEO-based surfactants. (Fig.S5) N_2 sorption results of samples shown in Table S2. (Fig.S6) FE-SEM results of samples shown in Table S2. (Fig.S7) Pseudo first-order rate constant determined from the linear graph of $\ln(C^o/C)$ versus time of meso-TiO_2 shown in Fig.7. (Table S3) Kinetic parameters of meso-TiO_2 for photo-degradation of RhB. See DOI: 10.1039/b000000x/

1 (a)W. Li, Z. Wu, J. Wang, A. A. Elzatahry and D. Zhao, *Chem. Mater.,* 2014, **26**, 287; (b) J. H. Pan, H. Dou, Z. Xiong, C. Xu, J. Ma and X. S. Zhao, *J. Mater. Chem.,* 2010, **20**, 4512; (c)S. W. Boettcher, J. Fan, C.-K. Tsung, Q. Shi and G. D. Stucky, *Acc. Chem. Res.,* 2007, **40**, 784.
2 (a) F. Schüth, *Chem. Mater.,* 2001, **13**, 3184; (b) R. Zhang, A. A. Elzatahry, S. S. Al-Deyab and D. Zhao, *Nano Today,* 2012, **7**, 344.
3 D. M. Antonelli and J. Y. Ying, *Angew. Chem., Int. Ed.,* 1995, **34**, 2014.
4 (a) D. L. Li, H. S. Zhou and I. Honma, *Nat. Mater.,* 2004, **3**, 65; (b) J. Lee, M. C. Orilall, S. C. Warren, M. Kamperman, F. J. Disalvo and

U. Wiesner, *Nat. Mater.* 2008, **7**, 222; (c) R. Liu, Y. Ren, Y. Shi, F. Zhang, L. Zhang, B. Tu and D. Zhao, *Chem. Mater.,* 2008, **20**, 1140; (d) R. Zhang, B. Tu and D. Zhao, *Chem. Eur. J.,* 2010, **16**, 9977; (e) W. Dong, Y. Sun, C. W. Lee, W. Hua, X. Lu, Y. Shi, S. Zhang, J. Chen and D. Zhao, *J. Am. Chem. Soc.,* 2007, **129**, 13894.

5 (a) H. Yoshitake, T. Sugihara and T. Tatsumi, *Chem. Mater.,* 2002**, 14**, 1023; (b) S. Y. Choi, M. Mamak, N. Coombs, N. Chopra and G. A. Ozin, *Adv. Funct. Mater.,* 2004, **14**, 335; (c) W. Zhou, F. Sun, K. Pan, G. Tian, B. Jiang, Z. Ren, C. Tian and H. Fu, *Adv. Funct. Mater.,* 2011, **21**, 1922; (d) E. L. Crepaldi, G. Soler-Illia, D. Grosso, F. Cagnol, F. Ribot and C. Sanchez, *J. Am. Chem. Soc.,* 2003, **125**, 9770; (e) B. Tian, H. Yang, X. Liu, S. Xie, C. Yu, J. Fan, B. Tu and D. Zhao, *Chem. Commun.,* 2002, 1824; (f) J. M. Yu, X. Wang and X. Fu, *Chem. Mater.,* 2004**, 16**, 1523; (g) H. S. Yun, K. Miyazawa, H. S. Zhou, I. Honma and M. Kuwabara, *Adv. Mater.,* 2001, **13**, 1377; (h) P. Yang, D. Zhao, D. I. Margolese, B. F. Chmelka and G. D. Stucky, *Nature,* 1998, **396**, 152; (i) P. D. Yang, D.Y. Zhao, D. I. Margolese, B. F. Chmelka and G. D. Stucky, *Chem. Mater.,* 1999, **11**, 2813; (j) G. Soler-Illia, A. Louis and C. Sanchez, *Chem. Mater.,* 2002, **14**, 750; (k) E. Beyers, P. Cool and E. F. Vansant, *J. Phys. Chem. B,* 2005, **109**, 10081.

6 (a) D. Chen, L. Cao, F. Huang, P. Imperia, Y.-B. Cheng and R. A. Caruso, *J. Am. Chem. Soc.,* 2010, **132**, 4438; (b) B. Smarsly, D. Grosso, T. Brezesinski, N. Pinna, C. Boissière, M. Antonietti and C. Sanchez, *Chem. Mater.,* 2004, **16**, 2948; (c) J. Zhang, Y. Deng, D. Gu, S. Wang, L. She, R. Che, Z.-S. Wang, B. Tu, S. Xie and D. Zhao, *Adv. Energy Mater.,* 2011,**1**, 241; (d) D. Feng, W. Luo, J. Zhang, M. Xu, R. Zhang, H. Wu, Y. Lv, A. M. Asiri, S. B. Khan, M. M. Rahman, G. Zheng and D. Zhao, *J. Mater. Chem. A,* 2013, **1**, 1591; (e) M. Nedelcu, J. Lee, E. J. W. Crossland, S. C. Warren, M. C. Orilall, S. Guldin, S. Huttner, C. Ducati, D. Eder, U. Wiesner, U. Steiner and H. J. Snaith, *Soft Matter,* 2009, **5**, 134; (f) A. H. Yuwono, Y. Zhang, J. Wang, X. H. Zhang, H. Fan and W. Ji, *Chem. Mater.,* 2006, **18**, 5876; (g) S. Sallard, M. Schröder, C. Boissière, C. Dunkel, M. Etienne, A. Walcarius, T. Oekermann, M. Wark and B. M. Smarsly, *Nanoscale,* 2013, **5**, 12316; (h) S. H. Ahn, W. S. Chi, D. J. Kim, S. Y. Heo and J. H. Kim, *Adv. Funct. Mater.,* 2013, **23**, 3901; (i) J. T. Park, J. H. Prosser, S. H. Ahn, S. J. Kim, J. K. Kim and D. Lee, *Adv. Funct. Mater*., 2013, **23**, 2193.

7 (a) E. J. W. Crossland, N. Noel, V. Sivaram, T. Leijtens, J. A. Alexander-Webber and H. J. Snaith, *Nature* 2013, **495**, 215; (b) K. Zimny, T. Roques-Carmes, C. Carteret, M. J. Stébé and J. L. Blin, *J. Phys. Chem. C,* 2012, **116**, 6585.

8 (a) D. C. Hurum, A. G. Agrios, K. A. Gray, T. Rajh and M. C. Thurnauer, *J. Phys. Chem. B,* 2003, **107**, 4545; (b) M. Yan, F. Chen, J. Zhang and M. Anpo, *J. Phys. Chem. B,* 2005, **109**, 8673; (c) L. Chen, B. Yao, Y. Cao and K. Fan, *J. Phys. Chem. C,* 2007, **111**, 11849; (d) D. Wang, D. Choi, Z. Yang, V. V. Viswanathan, Z. Nie, C. Wang, Y. Song, J.-G. Zhang and J. Liu, *Chem. Mater.,* 2008, **20**, 3435; (e) W. Yue, X. Xu, J. T. S. Irvine, P. S. Attidekou, C. Liu, H. He, D. Zhao and W. Zhou, *Chem. Mater.,* 2009, **21**, 2540.

9 (a) N. Satoh, T. Nakashima and K. Yamamoto, *Sci. Rep*., 2013**, 3**, 1959; (b) L. Robben, A.A. Ismail, S. J. Lohmeier, A. Feldhoff, D. W. Bahnemann and J. Buhl, *Chem. Mater*., 2012, **24**, 1268.

10 H. Shibata, T. Ogura, T. Mukai, T. Ohkubo, H. Sakai and M. Abe, *J. Am. Chem. Soc.,* 2005, **127**, 16396.

11 (a)J. Mühlebach, K. Müller and G. Schwarzenbach, *Inorg. Chem.,* 1970, **9**, 2381; (b) H. Ichinose, M. Terasaki and H. Katsuki, *J. Ceram. Soc. Jpn.*, 1996, **104**, 715.

12 (a)N. Murakami, Y. Kurihara, T. Tsubota and T. Ohno, *J. Phys. Chem. C* 2009, **113**, 3062; (b)W. Low and V. Boonamnuayvitaya, *J. Environ. Manage.,* 2013, **127**, 142; (c) D. Qian, Y. Li, Q. Zhang, G. Shi and H. Wang, *J. Alloys Compd.,* 2011, **509**, 10121.

13 H. Zhang and J. F. Banfield, *J. Phys. Chem., B* 2000, **104**, 3481.

14 A. Hagfeldt and M.Gratzel, *Chem. Rev.,* 1995, **95**, 49.

15 E. P. Barrett, L. G. Joyner and P. P. Halenda, *J. Am. Chem. Soc.,* 1951, **73**, 373.

16 (a) J. C. P. Broekhoff and J. H. de Boer, *J. Catal.,* 1967, **9**, 8; (b) J. C. P. Broekhoff and de J. H. Boer, *J. Catal.,* 1968, **10**, 153; (c) J. C. P. Broekhoff and J. H. de Boer, *J. Catal.,* 1968, **10**, 368.

17 D. Y. Zhang, D. Yang, H. J. Zhang, C. H. Lu and L. M. Qi, *Chem. Mater.,* 2006, **18**, 3477.

18 S. Yamada, Z. Wang, E. Mouri and K. Yoshinaga, *Colloid Polym. Sci.*, 2009, **287**,139.

19 M. S. Wong, E. S. Jeng and J. Y. Ying, *Nano Lett.,* 2001, **1**, 637.

20 Y. Wan, D. Zhao and Y. Shi, *Chem. Commun.,* 2007, 897.

21 (a) M. Kruk, *Acc. Chem. Res*. 2012, **45**, 1678; (b) D. Zhao, Q. Huo, J. Feng, B. F. Chmelka and G. D. Stucky, *J. Am. Chem. Soc.,* 1998, **120**, 6024.

22 G. Wanka, H. Hoffman and W. Ulbricht, *Macromolecules,* 1994, **27**, 4145.

23 R. Zana, *Colloids Surf., A* 1997, **123-124**, 27.

24 (a) W. Wang, W. Shan, H. Ru and N. Wu, *J. Mater. Chem.,* 2011, **21**, 12059; (b) W. Wang, W. Shan and H. Q. Ru, *J. Mater. Chem*., 2011, **21**, 17433; (c) W. Wang, W. J. Shan, H. Q. Ru, X. Y. Yue, J. Zhao, C. P. Zhang, B. Y. Zhao and S. Gao, *J. Sol-Gel Sci. Technol.,* 2012, **64**, 200.

25 (a) W. Wang, Y. Pang and S. Hodgson, *J. Mater. Chem.,* 2010, **20**, 8591; (b) X. Wang, J. M. Yu, C. Ho, Y. Hou and X. Fu, *Langmuir,* 2005, **21**, 2552.

26 (a) H. Ichinose, M. Terasaki and H. Katsuki, *J. Sol-Gel Sci. Technol.,* 2001, **22**, 33; (b) D. Qian, Y. Li, Q. Zhang, G. Shi and H. Wang, *J. Alloys Compd.,* 2011, **509**, 10121.

27 B. Ohtani, O.O. Prieto-Mahaney, D. Li and R. Abe, *J. Photochem. Photobiology A,* 2010, **216**, 179.

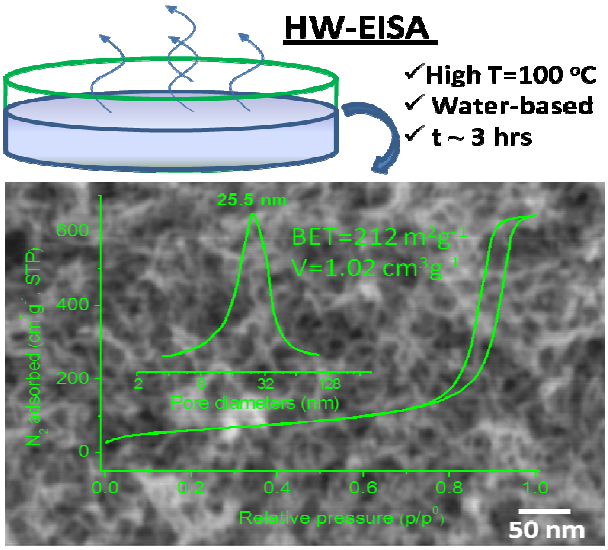

Through a high-temperature and water-based EISA (HW-EISA) approach, mesoporous TiO_2 with high surface areas (140-240 m^2g^{-1}), ultra-large mesopores (20-30 nm)/pore volumes (0.7-1.0 cm^3g^{-1}) and tuneable bi-crystallinity (anatase plus rutile) can be facilely prepared in a ternary templating system (peroxotitanic acid/P123/H_2O).